한국에너지공학회지(1999), 제8권 제1호
Energy Engg. J(1999), Vol. 8, No. 1, pp. 110~118

Numerical Analysis of the Chemical Injection Characteristics Using a Low Reynolds Number Turbulence Model

Byong Hoon Chang†, Chang Kyu Chung‡ and Han Rim Choi*

†*Mechanical Design Department, Junior College of Inchon*
‡*Chemical and Volume Control System Engineering, Korea Power Engineering Company, Inc.*
**Accident Analysis Group, Korea Power Engineering Company, Inc.*

Abstract — In order to protect the nuclear reactor coolant system from corrosion, lithium is injected into the coolant from the chemical injection tank. The present study investigates the chemical injection characteristics of the injection tank using a low Reynolds number turbulence model. Laminar flow analysis showed very little diffusion of the jet and gave incorrect flow and concentration fields. A disk located near the inlet of the injection tank was effective in mixing the chemical additives in the top portion of the tank, and significant reduction in injection time was obtained.

1. Introduction

The reactor coolant system of a pressurized-water reactor nuclear power plant is susceptible to corrosion from impurities such as dissolved oxygen, oxidizing species and chloride[1]. The impurities also increase the radiation level, and thus chemical control of the coolant system is essential in order to neutralize these effects[2]. The chemical control is performed by a volume control tank and chemical addition system. At coolant temperatures above 150°F, hydrogen is injected into coolant in the volume control tank to react with and remove the dissolved oxygen. At coolant temperatures below 150°F, hydrazine is injected in the chemical addition system to remove oxygen and to inhibit fluoride-induced corrosion.

Corrosion may also occur at lower pH caused by boron that is added to the coolant for the control of reactivity. The desired range of the pH of the coolant is maintained by controlling the lithium concentration in the chemical addition system. YongGwang 3&4 and Ulchin 3&4 nuclear power plants have the chemical addition system installed downstream of the CVCS (Chemical and Volume Control System) charging pump. This arrangement is advantageous in that the components upstream of the chemical addition system are free from contact by the high concentration chemical additives. But, the disadvantage of this arrangement is the requirement of a separate injection pump due to the high pressure downstream of the charging pump. Additional disadvantages are maintenance of the additional pump and a loss of chemical injection capability upon a pump failure. An alternative design is the installation of the chemical addition tank upstream of the CVCS charging pump. The advantages of this arrangement are that the need of a chemical injection pump and subsequently its maintenance are eliminated, and that the probability of the chemical injection failure is lowered. However, since the chemical additives come in contact with the components of the CVCS including the charging pump, there is a limitation on the maximum concentration of lithium in order to protect the system from a possible corrosion. In the present study, a numerical analysis has been performed in order to study the flow and chemical mixing characteristics of the proposed chemical addition tank to be installed upstream of the CVCS charging pump.

2. Analysis

It has been suggested that the maximum con-

centration of lithium be 600 ppm in order to protect the components of the CVCS from corrosion[2]. Based on this limitation, the maximum injection flow rate of lithium allowed was calculated as 2 gpm in an initial study[3]. Previous investigators[1,3,4] have performed laminar flow calculations for tank configurations of various height to diameter ratios, and the results showed that over 30% of the lithium remained in the tank of 11 gallons after 2 hours upon injection. In order to enhance mixing and expedite the injection process of the chemical additives, they performed laminar flow calculations with a disk placed at various locations in the tank. Their results[1,3,4] showed that 30% of the chemical additives remained in the tank at about 8 minutes after injection for a disk placed at 1/6H from the inlet. The role of the disk was to block the incoming fluid that has no chemical additives, and prevent the inflow with zero chemical concentration from simply exiting the tank without adequate mixing with the surrounding fluids. For a disk at 1/6H, it took about 1/2 hour to completely discharge the chemical additives from the tank. They performed numerical studies for other disk locations of 2/4H and 5/6H from the inlet and found that the disk placed at 1/6H gave the best results. Calculations with three disks located at 1/6H, 2/4H, and 5/6H did not show significant improvements over a single disk located at 1/6H from the inlet.

However, for jet Reynolds number exceeding 1000, the shear layer between the jet and the ambient fluid is turbulent[5]. Also, a jet is considered to be in transition regime for 1000<Re<3000, and fully turbulent for Re greater than 3000[6]. For the present problem, water is injected into the chemical addition tank through a pipe connected to the top, and the flow is like a jet issuing from a nozzle into a stagnant fluid. The jet Reynolds number based on 2 gpm is 6350, and the flow is in turbulent regime. In the present study, the flow field is calculated using a low-Reynolds number turbulence model. The widely tested Lam-Bremhorst low-Reynolds number k-ε turbulence model[7] below has been selected since it has been proved suitable also for prediction of transition[8,9]. The present problem is expected to have laminar, transition, and turbulent regimes, and the Lam-Bremhorst model should be suitable for the purpose. The governing equations have the general form as follows.

$$\frac{\partial}{\partial t}(\rho\phi)+\frac{\partial}{\partial x}(\rho u\phi)+\frac{1}{r}\frac{\partial}{\partial r}(r\rho v\phi)$$
$$=\frac{\partial}{\partial x}\left(\Gamma_\phi\frac{\partial\phi}{\partial x}\right)+\frac{1}{r}\frac{\partial}{\partial r}\left(r\Gamma_\phi\frac{\partial\phi}{\partial r}\right)+S_\phi \qquad (1)$$

where the effective diffusion coefficients and source terms are given in Table 1.

For the continuity equation, $\phi=1$, and $\Gamma_\phi=S_\phi=0$. The generation of the turbulence kinetic energy, G, is given by

$$G=\mu_t\left\{2\left[\left(\frac{\partial u}{\partial x}\right)^2+\left(\frac{\partial v}{\partial r}\right)^2+\left(\frac{v}{r}\right)^2\right]+\left(\frac{\partial u}{\partial r}+\frac{\partial v}{\partial x}\right)^2\right\} \qquad (2)$$

The turbulent viscosity, μ_t, is $c_\mu f_\mu \rho k^2/\varepsilon$, and the damping functions and related constants are given as

$$f_1=1+(0.05/f_\mu)^3,\ f_2=1-\exp(-R_t^2)$$
$$f_\mu=\{1-\exp(-0.0165\,R_y)\}^2,$$
$$R_y=k^{1/2}y/\nu,\ R_t=k^2/(\varepsilon\nu)$$
$$\sigma_k=1.0,\ \sigma_\varepsilon=1.3,\ c_\mu=0.09,\ c_1=1.44,\ c_2=1.92 \qquad (3)$$

The initial conditions were

$$u=0,\ v=0,\ c=1,\ k=0,\ \varepsilon=0 \qquad (4)$$

Table 1. Diffusion coefficients and source terms.

ϕ	Γ_ϕ	S_ϕ
u	$\mu+\mu_t$	$\frac{\partial}{\partial x}\left(\Gamma_u\frac{\partial u}{\partial x}\right)+\frac{1}{r}\frac{\partial}{\partial r}\left(r\Gamma_u\frac{\partial v}{\partial x}\right)-\frac{\partial P}{\partial x}$
v	$\mu+\mu_t$	$\frac{\partial}{\partial x}\left(\Gamma_v\frac{\partial u}{\partial r}\right)+\frac{1}{r}\frac{\partial}{\partial r}\left(r\Gamma_v\frac{\partial v}{\partial r}\right)-2\Gamma_v\frac{v}{r^2}-\frac{\partial P}{\partial r}$
k	$\mu+\frac{\mu_t}{\sigma_k}$	$G-\rho\varepsilon$
ε	$\mu+\frac{\mu_t}{\sigma_\varepsilon}$	$c_{\varepsilon1}f_1\frac{\varepsilon}{k}G-c_{\varepsilon2}f_2\rho\frac{\varepsilon^2}{k}$
c	$\frac{\mu}{S_c}+\frac{\mu_t}{\sigma_m}$	0

The inlet conditions used were uniform profiles with

$$u = u_{in},\ v = 0,\ c = 0 \tag{5}$$

and, the turbulence intensity of 0.5% and the profile of ε are given as follows.

$$k_{in} = 0.005\, u_{in}^2,\ \varepsilon_{in} = c_\mu k_{in}^{1.5}/(0.015\, d) \tag{6}$$

The wall boundary conditions were

$$u = 0,\ v = 0,\ \partial c/\partial x_i = 0,\ k = 0,\ \partial \varepsilon/\partial x_i = 0 \tag{7}$$

In the calculation of wall mass transfer rates in separated aqueous flow, Nesic *et al.*[10] found that use of the turbulent Schmidt number, σ_m, equal to 1.7 for $y^+ < 5$, and $\sigma_m = 0.9$ for $y^+ \geq 5$, gave better agreement of wall mass transfer rate with experimental data than using the simpler specification of $\sigma_m = 0.9$ throughout the computation domain. In the present problem, wall mass transfer rates are not significant, and the turbulent Schmidt number σ_m in the effective diffusivity for the species equation was assumed constant at 0.9.

The discretized equations were solved using PHOENICS[11]. The SIMPLEST algorithm[12] was used for the pressure-velocity coupling, and the integration in time was fully implicit, with the time step $\triangle\tau$ ranging from 2.3E-6 to 2.3E-5. The convective terms were approximated by the second-order, and bounded, TVD scheme proposed by Van Leer[13]. For each time step, the solutions were regarded as converged when R, the absolute residuals of the equations summed over all cells in the computational domain, defined as Eq. (8), divided by inlet flux became less than 0.1% for the continuity equation and 1% for other variables.

$$R = \sum_{j=1}^{m}\sum_{i=1}^{n} \left| a_p\phi_p - \sum a_l \phi_l - s \right| \tag{8}$$

The average concentration in the tank and the average concentration at each axial node location were also monitored, and the relative errors were smaller than 0.1% over 50 sweeps when the solutions were converged.

The computational grid was non-uniform with 44 nodes in radial and 96 nodes in axial directions for configurations with a disk located at x = 3/4H and 2/4H, and 44x97 for a disk placed at x=1/4H. Results obtained with approximately 60% more nodes showed that the computations were essentially free from numerical errors; concentration profiles were practically same for the two cases with maximum relative difference of about 0.5%. A computational grid of 35x58 was found adequate for the injection tank without a disk. Near the walls and the disk, at least 3 nodes were placed in the laminar viscous sublayer. The thickness of the mass transfer sublayer is suggested by Levich[14] as $\delta_m = \delta/Sc^{0.33}$ where δ is the laminar viscous sublayer. For the Schmidt number of 250 in the present problem, the mass transfer sublayer is about 1/6 of the hydrodynamic viscous sublayer. More refined grids should be placed near the solid boundaries in order to accurately solve the wall mass transfer rate. However, wall mass transfer rates are not relevant to the present problem.

3. Results

The computaion domain considered in the present analysis is schematically shown in Fig. 1. The tank configuration considered is for d/D = 0.1, b/D = 0.33, e/b = 0.24 and D/H = 0.47. Fluid with zero chemical concentration enters from the top of the tank and exits through the outlet located at the center of the bottom. Experimental data are not available for the present configuration, and a similar flow field of Taylor[15] was chosen to validate the code. Taylor[15] performed experiments for flow over an axisymmetric disk in a water tunnel, and the flow configuration was same as Fig. 1 except that the inlet diameter d is same as the pipe diameter D. Figure 2 shows comparison of the present calculations with the experimental data of Taylor[15] and the numerical results of McGuirk *et al.*[16] for a disk of 25% area blockage ratio and Re = 34,700. McGuirk *et al.* have used the high Reynolds number form of the Jones and Launder's $k-\varepsilon$ model[17]. Compared to the numerical results of McGuirk *et al.*, the computed profile near the pipe wall at x/R = 0.8 (here, x is the distance measured from the trailing edge of the disk) is rather flat, and that near the center is somewhat

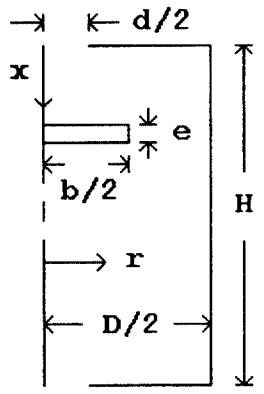

Fig. 1. The schematic diagram of computational domain.

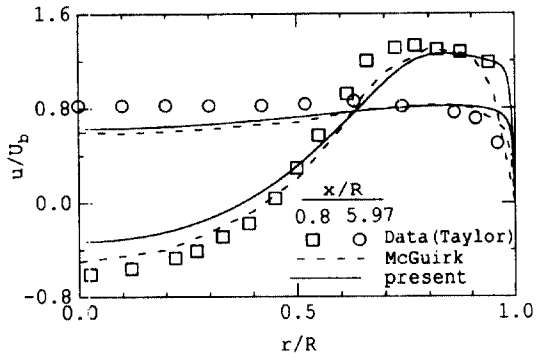

Fig. 2. Comparison of the axial velocity profiles.

underpredicted. However, there is a difference between the computational domain of McGuirk and that of the present study. The solution domain of McGuirk *et al.* extends from the trailing edge of the disk, and the measured experimental data in the annular gap were used as the inlet condition. Thus, the flow field before, and at the top of, the disk are not analyzed. In the present calculation, fully developed profiles of velocities and turbulence quantities obtained from pipe flow calculations were used as inlet conditions at 2 pipe diameters upstream of the disk, and the complete flow field around the disk is analyzed. The computational domain of the chemical injection tank contains a disk, and the purpose was to simulate the Taylor's experiment similar to the simulation of present problem of the chemical injection tank. The distance between the trailing edge of the disk and the outlet was set same as that of McGuirk *et al.* However, the outlet located at twice the distance of Mcguirk's calculation domain did not have any effect upstream, and the same results were obtained. Another difference is that the disk used in the experiment was sharp-edged, leading to larger radial velocities at the trailing edge of the disk, and stronger backflow is expected. On the other hand, the disk of the present calculation was chosen as rectangular, and the radial velocity towards the pipe wall at the trailing edge is smaller. Thus, a smaller recirculation zone and weaker back flow are expected behind the disk. Despite the differences in computational domain and inlet conditions, present results using the Lam Bremhorst model show good agreements with the experimental data and the numerical results of McGuirk *et al.*

The flow and concentration field were initially solved for the computation domain of Fig. 1 without any disk inside. The computed jet velocity profiles at x/d = 9.5, 14.3, 16.7, and 17.9 were compared with the self-similar jet profile[18] that occurs for x/d> 20 in Fig. 3. Although the computation domain extends only up to 21.3 d in the axial direction, the results near the outlet and away from the tank wall show good agreements with the experimental data. The computed velocity profiles about the side wall could not be compared due to the reverse flow.

Figure 4 shows the streamline plot for laminar flow at t = 30 seconds and those for turbulent flow analysis at t = 5 and 30 seconds. The ratio of the tank height to the tank radius is about 4.25, and the figures are presented somewhat compressed in the

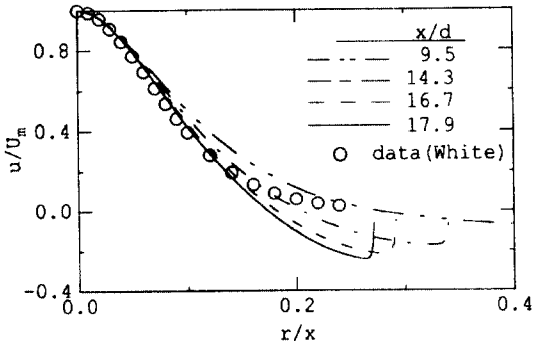

Fig. 3. Comparison of the axisymmetric turbulent jet with data.

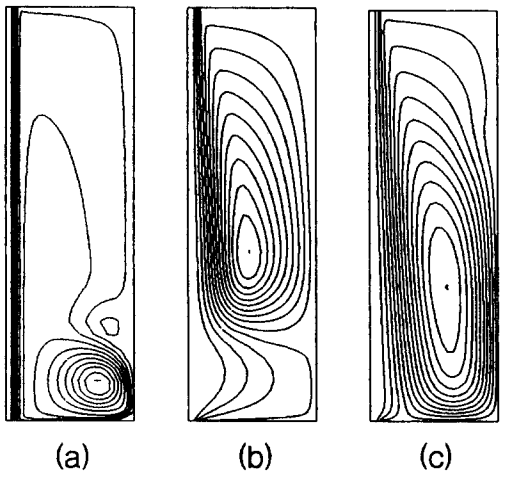

Fig. 4. Streamlines for (a) laminar flow analysis at t = 30 sec. (b) turbulent flow analysis at t = 5 sec. (c) turbulent flow analysis at t = 30 sec.

axial direction. The inlet is located at the top left-hand corner of the figures, and the outlet is at the bottom left-hand corner. Whereas the results for turbulent flow analysis show gradual spreading of the axisymmetric free jet, there is no noticeable diffusion of the jet into the surrounding fluid for the laminar flow analysis. The differences can be better observed in the three-dimensional contour plots of lithium concentration at t = 60 seconds shown in Fig. 5. The inlet is located at r = 0 and x = 0 in the figure, and the outlet is located at r = 0 and x = H. Fig. 5(a) shows that there is no noticeable diffusion of the jet into the surrounding fluid for the laminar flow analysis, and most of the injected flow with zero chemical concentration exits the tank without mixing with the surrounding fluid; the concentration in the tank remains close to 1 except the path of the injected flow around the centerline. A slight decrease in concentration can be observed in the lower part of the tank where there is a weak recirculation bubble as shown in Fig. 4(a). Concentration profile for turbulent flow analysis in Fig. 5(b) shows that effective mixing takes place and concentration is nearly below 0.75 in the bottom half of the tank. Concentration profile looks fairly flat in the bottom region of the tank, but this is due to the view angle, and there actually is a gradual increase of concentration from the centerline at r = 0 towards the

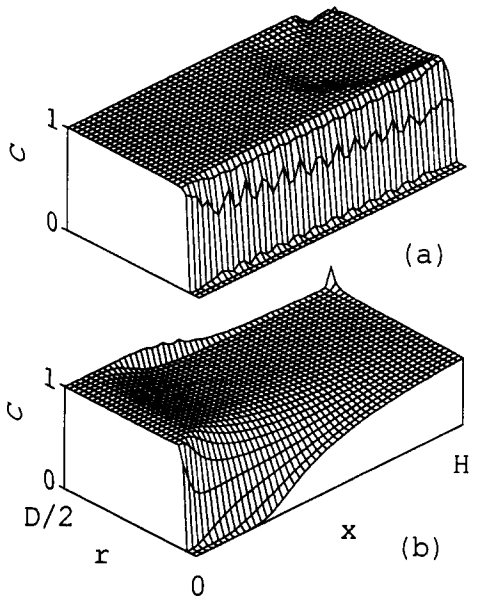

Fig. 5. Concentration profile without a disk at t = 60 sec. for (a) laminar flow analysis (b) turbulent flow analysis.

tank wall. Concentration is zero around the centerline only up to x≃0.25H. Assumption as laminar flow gives erroneous flow and concentration fields.

Figure 6 shows streamline plots at 5 seconds for a disk located at x = 3/4H, 2/4H, and 1/4H. The streamline plots at 60 seconds for the same disk locations are shown in Fig. 7. The jet impinges on

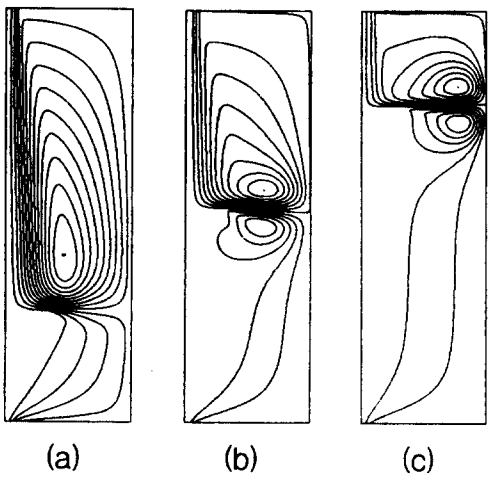

Fig. 6. Streamlines at t = 5 sec. with a disk at (a) x = 3/4H (b) x = 2/4H (c) x = 1/4H.

the disk, and a wall jet is formed along the disk in the radial direction. The second impingement occurs at the side wall and the flow separates into two recirculation bubbles. The transient plots show a gradual forming of a second recirculation bubble behind the disk (disk is not shown in the plot). The concentration fields for the injection tank with no disk at t = 30, 120, and 420 seconds are shown in Fig. 8. The concentration is 1 in the tank at t = 0, and the fluid without any chemical additives enters through the inlet at the top left-hand corner producing a sharp gradient in concentration. Gradual diffusion and mixing about the center can be observed. Figures 9, 10, and 11 show the concentration profiles for tank configurations with a disk placed at x = 3/4H, 2/4H, and 1/4H, respectively. Figure 11 shows that the chemical concentration in the top portion for x = 1/4H configuration decreases at a faster rate than those of other disk locations of 3/4H and 2/4H. As the fluid with relatively high velocity enters the tank, there is little mixing with the ambient fluid in the top portion around the inlet. Thus it takes longer to empty the top portion of the chemical additives. When a disk is placed closer to

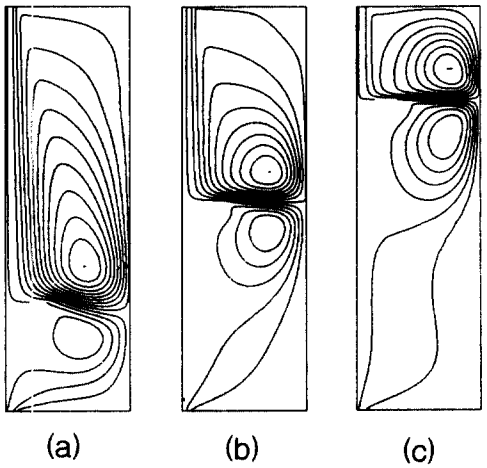

Fig. 7. Streamlines at t = 60 sec. with a disk at (a) x = 3/4H (b) x = 2/4H (c) x = 1/4H.

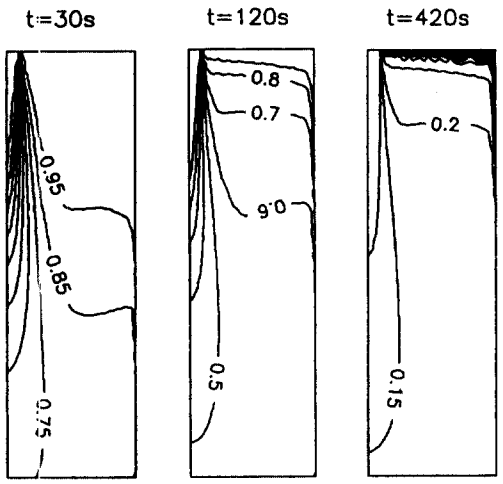

Fig. 8. Concentration profile without a disk for 30, 120, and 420 sec.

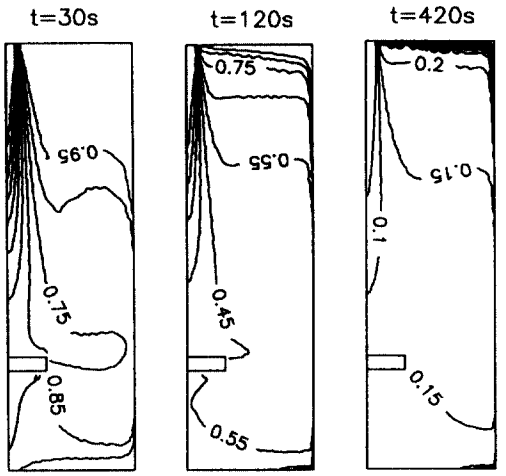

Fig. 9. Concentration profile with a disk at x = 3/4H for 30, 120, and 420 sec.

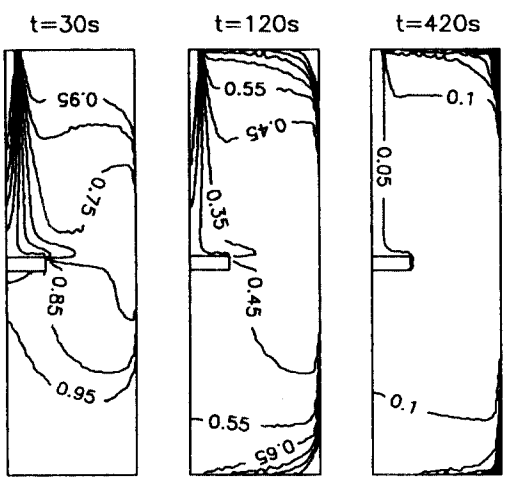

Fig. 10. Concentration profile with a disk at x = 2/4H for 30, 120, and 420 sec.

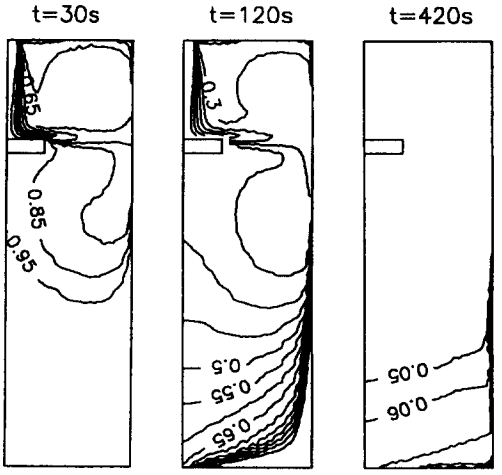

Fig. 11. Concentration profile with a disk at x = 1/4H for 30, 120, and 420 sec.

the inlet, the recirculation bubble becomes effective in mixing the inflow with the chemical additives in the top portion of the tank. Concentration profiles can be better observed in three-dimensional plots shown in Fig. 12. The three-dimensional plots are equivalent to the profiles in Figures 9, 10, and 11 for t=30 seconds.

Figure 13 shows the average concentrations of lithium in the tank for time up to 10 minutes. All the results are obtained with turbulent analysis except the solid line of the ideal case and the laminar flow result without a disk. The laminar analysis produces very little diffusion of the jet into the surrounding fluid as shown in Fig. 5, and over 85% of the lithium remains in the tank at 10 minutes. Laminar flow analysis performed with a disk placed along the centerline of the tank gave significant reduction in the average concentration, but there was very little spreading of the wall jets that are developed on the disk and the tank wall. The resulting flow and concentration fields were incorrect, and the effects of the disk for the laminar flow became too exaggerated. The straight solid line is the lowest possible average concentration with time; it is obtained assuming the solution is evenly pushed out of the tank with the speed of 2 gpm/ cross section area of tank. Except for the laminar flow calculation, the average concentrations for all the turbulent cases follow the straight line initially,

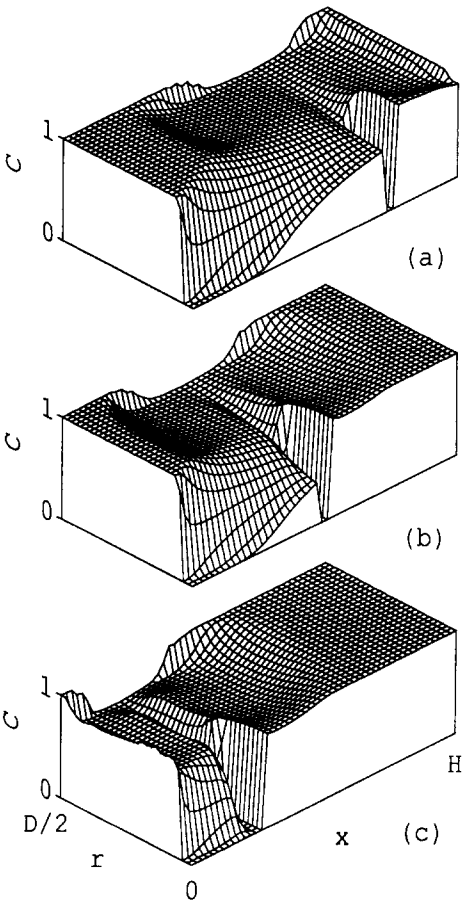

Fig. 12. Concentration profiles at t = 30 sec. with a disk at (a) x = 3/4H (b) x = 2/4H (c) x = 1/4H.

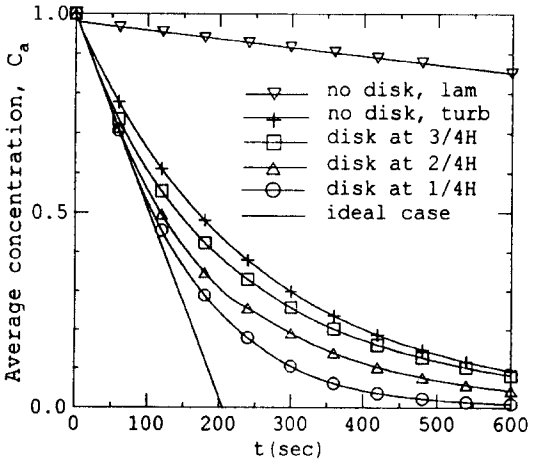

Fig. 13. Average concentration of lithium versus time.

since the fluid near the outlet is simply pushed out of the tank at the start of injection. When the disk is placed closer to the inlet, the recirculation bubble becomes effective in mixing the inflow with the chemical additives in the top portion of the tank. Furthermore, the chemical additives in the lower part of the tank that are unmixed with the incoming fluid are simply pushed out of the tank for a longer period at the begining of injection. The configuration with a disk at x = 1/4H gives the best performance; less than 1% of the lithium remains in the tank at 10 minutes. The concentration tapers off with time for all cases, and the effects of the disk become smaller. However, the disk is to be designed with four support legs, and the actual top and bottom of the tank are supposed to be partly spherical in shape. Thus, the actual mixing process is expected to be more efficient than indicated by the results of the present calculation.

4. Conclusion

The flow and mixing characteristics of the chemical injection tank to be installed upstream of the CVCS charging pump are investigated using the Lam-Bremhorst low-Reynolds number turbulence model. Modeling the problem as a laminar flow gave incorrect concentration profiles due to negligible diffusion of the jet. Turbulent flow analysis showed that efficient mixing with the chemical additives occur as the axisymmetric turbulent free jet spreads in the tank. Significant reduction in injection time was obtained with a disk located closer to the inlet of the tank. More efficient mixing and further reduction of injection time is expected for an actual design with four support legs.

Nomenclature

b	disk diameter
c	concentration
c_μ, c_1, c_2	turbulence model constants
d	tank inlet and outlet diameter
D	tank diameter
f_μ, f_1, f_2	turbulence model functions
H	tank height
k	turbulence kinetic energy [J/kg]
l	neighboring grid points
p	grid point under consideration
r	radial coordinate
R	D/2, or residual
Re	Reynolds number, $\rho u_b d/\mu$
R_k	turbulence Reynolds number, $k^2/(\varepsilon \nu)$
R_y	turbulence Reynolds number, $k^{1/2} y/\nu$
s	source
t	time
u	axial velocity [m/s]
v	radial velocity [m/s]
x	axial coordinate
ρ	density [kg/m^3]
μ	viscosity [kg/(m · s)]
ν	kinematic viscosity [m^2/s]
ϕ	general conserved property
ε	turbulence dissipation rate [J/(kg · s)]
α	thermal diffusivity [m^2/s]
σ_k	diffusion Prandtl number for turbulence energy
σ_ε	diffusion Prandtl number for dissipation rate
τ	non-dimensional time, $t\alpha/(d/2)^2$

Subscript

a	average
b	bulk
m	maximum, or mass
t	turbulent values

References

1. Chang, K.S. and Park, B.H.: "A Numerical Study on Mixing Characteristics of the Chemical Injection Tank", Journal of the Korean Nuclear Society, 29(1), 58-67 (1997).
2. Chemistry Design Guide for UCN 3&4, N0291-FS-CG110, KAERI (1993).
3. Park, B.H.: "Design Optimization of Chemical Addition System Using Numerical Method", Internal Report, KAERI (1996).
4. Park, B.H., Kim, E.K., Kim, Y.H., Ko, Y.S. and Chang, K.S.: "Analysis of Injection Time for Chemical Injection Tank Using Numerical Analysis", Proceedings of the Korean Nuclear Society Spring Meeting, Cheju, Korea, 55-60 (1996).

5. Womac, D.J., Ramadhyani, S. and Incropera, F.P.: "Correlating Equations for Impingement Cooling of Small Heat Sources With Single Circular Liquid Jets", Journal of Heat Transfer, 115, 106-115 (1993).
6. Gauntner, J.W., Livingood, J.N.B. and Hrycak, P.: "Survey of Literature on Flow Characteristics of a Single Turbulent Jet Impinging on a Flat Plate", NASA TN D-5652 (1970).
7. Lam, C.K.G. and Bremhorst, K.: "A Modified Form of the $k-\varepsilon$ Model for Predicting Wall Turbulence", Journal of Fluids Engineering, 103, Sep., 456-460 (1981).
8. Schmidt, R.C. and Patankar, S.V.: "Prediction of Transition on a Flat Plate Under the Influence of Free-Stream Turbulence Using Low-Reynolds Number Two-Equation Turbulence Models", ASME Paper 87-HT-32, 1-9 (1987).
9. Yang, L. C., Asako, Y., Yamaguchi, Y. and Faghri, M.: Numerical Prediction of Transitional Characteristics of Flow and Heat Transfer in a Corrugated Duct, J. of Heat Transfer, 119, 62-69 (1997).
10. Nesic, S, Postlethwaite, J. and Bergstrom, D.J.: Calculation of Wall-Mass Transfer Rates in Separated Aqueous Flow Using a Low Reynolds Number $k-\varepsilon$ model, Int. J. Heat Mass Transfer, 35, 1977-1985 (1992).
11. CHAM, Bakery House, 40 High Street, Wimbledon SW19 5AU, England.
12. Spalding, D.B.: Mathematical Modelling of Fluid-Mechanics, Heat-Transfer and Chemical-Reaction Processes: A Lecture Course, HTS/80/1, Imperial College of Science and Technology, Mechanical Engineering Department, London, England (1980).
13. Van Leer, B.: "Towards the Ultimate Conservative Difference Scheme II", J. Comp. Phys., 14, 361-370 (1974).
14. Levich, V.: Physicochemical Hydrodynamics, Prentice-Hall, Englewood Cliffs, NJ, pp. 144-154 (1962).
15. Taylor, A.M.K.P.: "Confined, Isothermal and Combusting Flows Behind Axisymmerical Baffles", Ph. D. Thesis, University of London (1981).
16. McGuirk, I.J., Taylor, A.M.K.P. and Whitelaw, J.H.: "The Assessment of Numerical Diffusion in Upwind Difference Calculation of Turbulent Recirculating Flows", Turbulent Shear Flows 3, 206-224, Springer-Verlag (1982).
17. Jones, W.P. and Launder, B.E.: "The Prediction of Laminarization With a Two-equation Model of Turbulence", Int. J. Heat Mass Transfer, 15, 301-314 (1972).
18. White, F.M.: Viscous Fluid Flow, McGraw-Hill, Inc. (1991).